Applied Thermal Engineering 235 (2023) 121402

Contents lists available at ScienceDirect

Applied Thermal Engineering

journal homepage: www.elsevier.com/locate/apthermeng

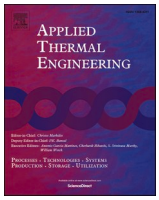

Research Paper

Investigating the efficiency of a novel combined Direct/Indirect thermal management system in optimizing the thermal performance of a new generation 46800-type LIB pack

Mahdi Tousi [a], Amirhosein Sarchami [b], Mohammad Najafi [a,*], Kishan Bellur [b]

[a] Department of Mechanics, Electrical Power and Computer, Science and Research Branch, Islamic Azad University, Tehran, Iran
[b] Department of Mechanical and Materials Engineering, University of Cincinnati, Cincinnati, OH, USA

ARTICLE INFO

Keywords:
Lithium-ion battery
Battery thermal management system
Direct/indirect liquid-cooled system
46800-type battery

ABSTRACT

Although the 46800-type Li-ion batteries have superior attributes, including high driving range, energy density, and fast charging capability, it is plagued by higher heat generation during discharge impacting performance, efficiency, and lifespan. To address this problem, a novel thermal management system is proposed utilizing direct/indirect liquid cooling with water, CuO nanofluid, and HFE-7100. Meshed separator plates are developed in the direct cooling channel to improve thermal uniformity and mitigate hot spots on LIBs. The numerical evaluation considers effects such as C-rate, coolant, separator wall, flow rates, flow direction, and ambient temperature on the thermal performance of the LIB pack. During a 3C discharge operation, compared to 1C, the LIB pack experiences a 7 °C increase in maximum temperature and a 4.1 °C temperature difference. However, with a 4% CuO nanofluid, these values decrease by 4.9 °C and 3 °C respectively, compared to water. A circular meshed separator wall improved the thermal performance of the battery pack by 22.7% compared to the non-wall condition. The inflow velocities of the direct and indirect cooling channels are increased from 0.2 to 0.3 m/s and from 0.1 to 0.2 m/s, respectively, which led to the 11.5% enhancement of the LIB pack's thermal efficiency. Finally, the thermal performance of the proposed cooling system is assessed by considering various ambient temperatures ranging from 25 °C to 40 °C for the LIB pack. The results indicated that the optimized cooling system can maintain the maximum temperature of the LIB pack below 40 °C, even at an ambient temperature of 35 °C.

1. Introduction

In recent years, the decline of internal combustion engine (ICE) vehicles has been driven by their harmful emissions and significant fossil fuel consumption [1]. Consequently, various alternatives like electric vehicles (EVs), plug-in hybrid electric vehicles (PHEVs), hydrogen fuel-cell vehicles (FCEVs), and more have emerged [2–5]. Among these alternatives, EVs show great promise, leading manufacturers to focus on designing eco-efficient EVs, with Lithium-ion batteries (LIB) being the most advantageous energy storage system due to their high power, stability, long lifespan, and energy density [6,7]. However, improvements are required, especially in LIB pack cooling, cost, driving range, and charging time. Optimized temperatures of the LIB packs should be 25 °C – 40 °C for optimal performance and the thermal non-uniformity of the LIB package should be maintained under 5 °C [8]. High or low temperatures can negatively impact LIB efficiency, with low temperatures affecting ionic conductivity and high temperatures causing thermal runaway and capacity fading [9–11]. To address these challenges, an effective battery thermal management system (BTMS) is crucial to regulate maximum temperatures and ensure temperature uniformity during charging and discharging operations, especially in fast charging/discharging conditions [12].

In general, BTMS can be classified into two main methods: active [13,14], and passive [15,16]. In the past decade, researchers have introduced several active and passive methods [17,18]. Among these cooling systems, the liquid-cooling strategy as an active method has emerged as a highly promising choice compared to other strategies such as air cooling, heat pipe, and phase change material (PCM) due to the superior thermal conductivity and heat capacity of liquids [19,20].

* Corresponding author at: Room 507, Department of Mechanics, Electrical Power and Computer, Science and Research Branch, Islamic Azad University, Tehran, Iran.
E-mail address: Najafi@srbiau.ac.ir (M. Najafi).

https://doi.org/10.1016/j.applthermaleng.2023.121402
Received 11 June 2023; Received in revised form 8 August 2023; Accepted 17 August 2023
Available online 19 August 2023

Nomenclature

List of symbols

C_{1-3}	Model constants
C_p	Specific heat ($Jkg^{-1}K^{-1}$)
C_μ	Constant
g	Gravitational acceleration (ms^{-2})
G_k	Kinetic energy turbulence generation (mean velocity gradients)
G_{buo}	Kinetic energy turbulence generation (buoyancy)
h	Heat transfer coefficient ($Wm^{-2}K^{-1}$)
I	Current (A)
K	Thermal conductivity ($Wm^{-1}K^{-1}$)
P	Pressure (Pa)
Q	Heat (W)
$\dot{Q}$	Volumetric heat generation rate (Wm^{-3})
R	Resistance (Ω)
Re	Reynolds number
S_ε	User-defined source term
S_M	Momentum source
T	Temperature (°C)
t	Time (s)
U	Voltage (V)
u	Velocity vector (ms^{-1})
V	Volume (m^3)

Greek symbols

μ	Dynamic viscosity ($kgm^{-1}s^{-1}$)
ρ	Mass density (kgm^{-3})
∇	Gradient operator

Abbreviations

BTMS	Battery thermal management system
CFD	Computational fluid dynamics
C-rate	Current charge/discharge rate
DI-water	Deionized water
DOD	Depth of discharge
CVM	Control volume method
EV	Electrified vehicle
FCEV	Fuel cell electrified vehicle
LCP	Liquid cold plate
LIB	Lithium-ion battery
NCM	$Li_xNi_{0.33}Co_{0.33}Mn_{0.33}O_2$
PCM	Phase change material
PHEV	Plug-in hybrid electric vehicle
SOC	State of charge
TMS	Thermal management system

Subscripts and superscripts

b	Battery
c	Coolant
dr	Drift
eff	Effective
gen	Generation
i	Battery component
ir	Irreversible
k	Secondary phase
m	Mixture
OCV	Open circuit voltage
P	Nanoparticle
re	Reversible

Liquid-cooled systems are categorized into two methods: indirect-based and direct-based. In indirect-based cooling systems such as liquid cold plate (LCP) or cooling channel, the coolant does not contact the LIB surfaces [21]. Pulugundla et al. [22] examined how different sizes and configurations of cold plate channels affect the overall thermal performance of a liquid-cooled BTMS, which utilized variable heat load from 21700-type LIB cells. The findings indicate that the performance of the LCP relies on both pressure drop and heat transfer coefficient. Sarchami et al. [23] used the novel stair/wavy types cooling channels based on Alumina nanofluid to ameliorate the thermal behavior of the 18650-type battery pack. They concluded that under the 5C fast discharging condition, with an environmental temperature of 25 °C, their proposed BTMS utilizing a 2% volume fraction of Alumina nanofluid and an inflow velocity of 0.5 m/s, effectively maintained the maximal temperature of the LIB pack below 33.5 °C. Liu et al. [24] used the conventional serpentine LCP which combined with the intersecting channels to improve the efficiency of the indirect-based liquid-cooled BTMS for prismatic LIBs. Their results indicated that adding intersecting channels notably improves the thermal performance of the battery pack. Designing an efficient and practical cooling channel based on the indirect technique is the most debated topic among the authors. Tousi et al. [25] investigated the thermal behavior of a 18650-format LIB pack which has an innovative nanofluid-cooled BTMS. They numerically analyzed the highest temperature and temperature non-uniformity of the battery pack at high discharge current rates such as 3C, 5C, and 7C. Their findings suggested that there is a direct correlation between the utilization of a high discharge C-rate and the increase in the overall temperature of the LIB pack. Also, the outcomes illustrated that the thermal performance of the LIB pack was improved by increasing the volume fraction of the nanofluid and its inflow velocity.

In contrast to the indirect-based cooling strategy, the direct-based method has a higher heat transfer behavior, which is useful for fast discharging and charging conditions [26]. A numerical study was conducted by Wang and Wu [27] to propose a new HFE-7000 immersion cooling system BTMS to evaluate the temperature change of the 18650-type LIB package. The result showed that the maximum temperature of the LIB pack is directly related to the inlet velocity of the coolant. To meet the requirement for the long-range and high safety of EVs, Wu et al. [28] proposed a direct-based cooling system BTMS. They used silicone oil to obtain an effective cooling system due to the excellent safety and high integration ratio. The results indicated that the maximum temperature and temperature difference of an 18650-type battery pack employing a direct cooling system are merely 20% to 30% of those observed in the indirect cooling system. Hong et al. [29] investigated the performance of a novel direct two-phase refrigerant (R134a) cooling system for lithium-ion batteries in electric vehicles. Results indicated that under superheat conditions, the maximum cell temperature and temperature difference increased among the LIBs near the module outlet. Furthermore, Dubey et al. [30] compared direct and indirect cooling systems for 21700-type LIB packs. The results indicated that the direct cooling system, which utilized a dielectric coolant (HFE-7500) with low specific heat and thermal conductivity, did not substantially improve the temperature uniformity of the LIB pack when compared to the indirect cooling system, which used a mixture of water and ethylene glycol.

Recently, the combined cooling methods, which integrates any combination of active and/or passive methods, have been introduced to further enhance the thermal efficiency of the battery pack compared to previous single methods [31,32]. Kiani et al. [33] experimentally investigated the cooling behavior of two pouch LIBs which integrated with nanofluid-cooled and PCM-based systems. They used nanofluids (Al_2O_3, CuO, and AgO) to improve heat transfer and enhance thermal

performance of two film heaters as substitutes for LIBs. Results demonstrated 23.8%, 40.5%, and 45.2% improvements with Al_2O_3, CuO, and AgO compared to pure water, respectively. Also, the results depicted that the temperature non-uniformity of the LIBs does not exceed 5 °C. A novel combined BTMS using heat pipes and a liquid-cooling plate is proposed by He et al. [34]. They numerically analyzed the impact of four aluminum sheet parameters such as height, thickness, covering angle to battery, and covering angle to heat pipe on LIB pack temperature distribution. Results showed optimal values for maximum temperature (37.58 °C) and temperature difference (3.67 °C) during 3C discharge. A thermal management system combining mini-channel liquid cooling and air cooling is proposed by Yang et al. [35] for 18650-type lithium-ion battery modules. Effects such as water flow rate, cooling tube and mini-channel quantity, tube space, flow direction, and spacer combination are investigated using computational fluid dynamics. Their results showed that even in the best-case scenario, the battery module experiences high temperature non-uniformity, and hot spots are emerged, especially at the outlet sections. Hence, it is well established that both indirect, direct as well as combined cooling systems, are effective in cooling lithium-ion batteries. However, there are challenges in achieving optimal thermal management due to potential limitations in design and configuration. Certain areas within the battery pack may not receive adequate cooling, leading to localized hotspots and temperature variations. Development of an innovative combined cooling system that can effectively tackle these concerns, especially in the new 46800-type LIB packs, is an immediate need.

In the present numerical investigation, an innovative combined direct/indirect liquid-cooled system for the conventional 46800-format batteries is presented to improve the thermal performance of the LIB pack. The LIB pack has 20 46800-format batteries, novel indirect/direct cooling channels, and copper separator plates (Fig. 1). The proposed cooling system is based on two liquid cooling strategies (direct and indirect). The working fluids for direct and indirect channels are HFE-7100, which is an engineered dielectric fluid and CuO nanofluid, respectively. Separator plates with meshed structures are implemented to improve the mixing effect in the direct cooling channel and thermal uniformity of the LIB pack; different mesh shapes (including circular, triangular, and square) are investigated. In this study, the influences of constant discharge C-rates (1, and 3), the volume fraction of CuO nanofluid (2%, and 4%), inflow velocity of channels, the shape of mesh in separator plates, and environmental temperature on the thermal behavior of a new 46800-type LIB pack are analyzed. The major purpose of this investigation is to optimize pathways to decrease the maximum temperature and temperature non-uniformity of the new generation 46800-type battery pack throughout the fast discharging condition using the combined cooling method. To ensure even distribution of the heat generated and transferred by LIBs, four indirect cooling channels have been designed, positioned both above and below each row of batteries. This integration effectively manages the heat within the batteries.

2. Numerical models

This section presents the numerical models of a novel liquid-cooled system employing the dielectric fluid (HFE-7100) and CuO nanofluid. Therefore, battery pack, nanofluid, and BTMS models are discussed in the following sub-sections.

2.1. Battery pack model

In this study, a new combined liquid indirect/direct cooling system for a new generation 46800-type LIB pack is proposed. Fig. 1 depicts the schematic of Li-ion battery pack with the indirect/direct cooling channels. Based on the mentioned figure, the LIB pack consists of twenty 46800-type Li-ion batteries. The LIB's technical, thermal, and physical parameters are tabulated in Table 1. The estimated energy density, as indicated in Table 1, is calculated from the total capacity of each cell, representing the actual capacity observed during real-world usage.

In the present investigation, the proposed cooling system manages and controls the peak temperature and particularly temperature non-uniformity of the battery pack in acceptable working temperature ranges, which are 25 °C – 40 °C, and less than 5 °C, respectively. As can be seen in Fig. 1, all LIBs are completely immersed in the dielectric fluid (HFE-7100) except for their negative and positive tabs. All battery cells are placed in an aligned arrangement that has fixed 20, and 40 mm

Table 1
Technical and thermo-physical parameters of 46800-type battery [36–39].

Parameter	Amount	Parameter	Type/Amount
Total Capacity,Ah	~ 26.1	Anode material	Graphite
Nominal Voltage,V	3.7	Cathode material	Nickel-Cobalt-Manganese (NCM)
Energy Density,$Whkg^{-1}$	272–296	Electrolyte material	Lithium salt ($LiPF_6$)
Mass,g	355	Density ρ,kgm^{-3}	2375.7
Height,mm	80	Specific heat C_p, $Jkg^{-1}K^{-1}$	1725
Diameter,mm	46	Thermal conductivity (axial - radial) k, $Wm^{-1}K^{-1}$	3.2 – 0.96

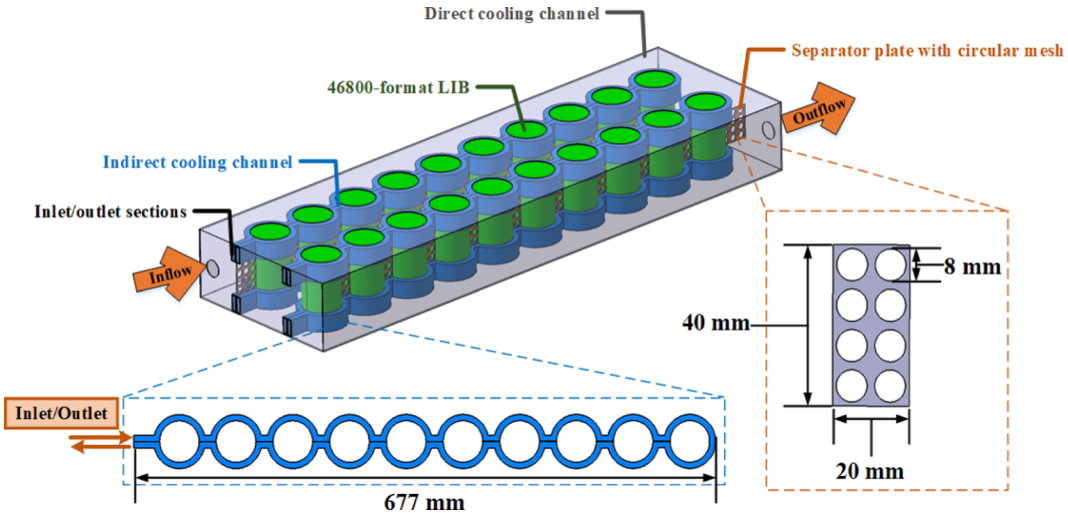

Fig. 1. Schematic of 46800-type LIB pack with the novel combined liquid-cooled battery thermal management system.

intervals between each other in a row and column, respectively. This study employs conventional 46800-format LIBs with a cylindrical structure containing Nickel-Cobalt-Manganese (NCM) as the cathode.

2.2. Coolant model

The working fluid that flows in the direct and indirect cooling channels are HFE-7100 and CuO nanofluid with 2%, and 4% volume fractions. The base fluid of the CuO nanofluid is water. The 3 M™ Novec™ 7100 engineered fluid is an exclusive hydrofluoroether (HFE) with distinct characteristics that make it exceptionally desirable for a wide array of applications and industries. These range from thermal management in semiconductor manufacturing to using it for direct cooling in data centers. The thermal properties of the HFE-7100, water, and CuO nanoparticles are indicated in Table 2.

Coolant features are the most important parameters in liquid cooling systems for both direct and indirect liquid cooling methods to manage thermal efficiency. Based on the thermal properties of the coolants, numerical calculations are conducted for different coolant domains. It should be noted that HFE-7100 is an engineered dielectric fluid, introduced to the direct cooling systems of electronic devices. This coolant has been used due to its advantages such as low viscosity, non-flammable, non-toxic, high boiling point (61 °C), and availability in large amounts. In addition, HFE-7100 has better thermal behavior in comparison with other dielectric fluids because of its high thermal conductivity and heat capacity [26]. Due to its high dielectric strength, HFE-7100 is well-suited for employing a direct cooling system in electronic devices as it effectively prevents the occurrence of any possible short-circuits [42]. Furthermore, the selection of CuO nanofluid is based on its various advantages, including enhanced thermal conductivity, compatibility, and stability of nanoparticles [43]. In the following subsections, the governing equations for single-phase coolants (water and HFE-7100) and two-phase fluid (CuO nanofluid) with different volume fractions are presented.

2.3. Governing equations

To carefully evaluate the thermal efficiency of the battery pack during the discharge operation, a thermal model (lumped treatment) [44,45] is applied to the 46800-type batteries. According to this thermal method, batteries are considered as a uniform body, and the internal temperature variation of cells is not considered. Hence, the thermal properties of the LIB including axial/radial thermal conductivities, density, and specific heat are calculated based on the equivalent equations. Because of variations in material composition along different directions, the cylindrical LIB exhibits distinct axial and radial thermal conductivities. As a result, the thermal model considers the thermal conductivity to be anisotropic [46].

$$K_a = \frac{\sum_i L_i k_i}{\sum_i L_i} \tag{1}$$

$$K_r = \frac{\sum_i L_i}{\sum_i L_i / k_i} \tag{2}$$

$$\rho = \frac{\sum_i \rho_i C_i V_i}{V_i C_p} \tag{3}$$

Table 2
Thermal properties of water, HFE-7100, and CuO nanoparticles [40,41].

Property (unit)	Water	Hydrofluoroether (HFE-7100)	CuO
ρ (kgm^{-3})	997.1	1510	6500
$C_p (Jkg^{-1}K^{-1})$	4179	1170	540
$k(Wm^{-1}K^{-1})$	0.613	0.069	18.0

$$C_p = \frac{1}{\rho_i} \frac{\sum_i \rho_i C_i V_i}{\sum_i V_i} \tag{4}$$

in which, K_a, K_r, V_i, C_i, ρ_i, and L_i denote the axial and radial thermal conductivities, as well as the volume, specific heat, density, and thickness of component "i" in a battery cell. The subscript "i" pertains to the LIB component. Based on the above equations (Eqs. 1–4) and physical parameters of 46800-type LIB, the equivalent thermal properties are calculated (Table 1).

This investigation is conducted using computational fluid dynamics (CFD) to assess the thermal behavior of the BTMS. The entire BTMS consists of different domains such as LIBs, aluminum indirect/direct cooling channels, and coolants. For simplicity, several numerical assumptions are made:

- The radiation heat transfer is neglected because of the low temperature difference between the ambient and LIB surface, and the effective heat transfer approaches are conduction and convection throughout the process. Furthermore, the consideration of thermal contact resistance between the channels and the LIB cells are neglected.
- All coolants are Newtonian, incompressible, and single-phase; however, CuO nanofluid has been simulated by using the mixture strategy.
- During the discharge operation of a Li-ion battery, the thermal power changes transiently due to variations in the internal resistance, current flow, and energy conversion processes, leading to dynamic fluctuations in heat generation within the battery. The thermal power of each battery undergoes transient fluctuations and is utilized during the discharge process by evaluating the variables and establishing customized functions.
- The thermal conductivity of LIBs is constant during the process due to the winding structure of the LIBs. Also, it is assumed that the density and specific heat are constant throughout the operations.
- The heat generation of the LIBs is from the core body of the cells and other parts of LIBs do not generate heat.

According to the assumptions, the governing equations such as continuity, momentum, and energy are presented for every component in the BTMS. The continuity, momentum, and energy equations of single-phase coolants (water/HFE-7100) are expressed as:

$$\nabla . \vec{u}_c = 0 \tag{5}$$

$$\rho_c \frac{\partial \vec{u}_c}{\partial t} + \left(\vec{u}_c . \nabla \right) \vec{u}_c = -\nabla p + \mu_c \nabla^2 \vec{u}_c + \rho_c \vec{g} \tag{6}$$

$$\frac{\partial T_c}{\partial t} + \left(\vec{u}_c . \nabla \right) T = \frac{K_c}{\rho_c C_p} \nabla^2 T_c \tag{7}$$

Both water and CuO nanofluids exhibit laminar flow regimes in the indirect cooling channels. However, in the direct cooling channel employing HFE-7100, the flow regime is turbulent, necessitating the use of the realizable k-ε model. This model is known for its strengths in providing reasonably accurate results across a wide range of flows and its proven ability to analyze heat transfer and fluid streams [27]. The equations for turbulent kinetic energy and eddy viscosity are denoted in Eqs. (8) and (9), respectively.

$$\frac{\partial \rho k}{\partial t} + \nabla \hat{A} \cdot \left[\rho \vec{V} k \right] = \nabla \hat{A} \cdot \left[\left(\mu + \frac{\mu_t}{\sigma_k} \right) \nabla k \right] + G_k + G_{buo} - \rho \varepsilon - Y_M + S_M \tag{8}$$

$$\frac{\partial \rho \varepsilon}{\partial t} + \nabla \hat{A} \cdot \left[\rho \vec{V} \varepsilon \right] = \nabla \hat{A} \cdot \left[\left(\mu + \frac{\mu_t}{\varepsilon_k} \right) \nabla \varepsilon \right] + C_1 \frac{\varepsilon}{k} (G_k + C_3 G_{buo}) - C_2 \rho \frac{\varepsilon^2}{k} + S_\varepsilon \tag{9}$$

The turbulent (or eddy) viscosity is calculated as presented in Eq.

(10):

$$\mu_t = \rho C_\mu \frac{k^2}{\varepsilon} \tag{10}$$

where C_{1-3}, C_μ, G_k, G_{buo}, S_ε, S_M are model constants, kinetic energy turbulence generation (mean velocity gradients), kinetic energy turbulence generation (buoyancy), source term, and momentum source, respectively.The energy equations of LIBs (Eq. (11)) and other solid components (Eq. (12)) like cooling channels, and separator walls are given by:

$$\frac{\partial}{\partial t}\left(\rho_b C_{p,b} T_b\right) = \nabla \bullet \left(K_b \nabla T_b\right) + \dot{Q}_b \tag{11}$$

$$\frac{\partial}{\partial t}\left(\rho C_p T\right) = \nabla \bullet \left(K \nabla T\right) \tag{12}$$

in which, K_b, t, $\dot{Q}_b$, $C_{p,b}$, T_b, and ρ_b represent the thermal conductivity, time, volumetric heat generation rate of batteries, specific heat of LIBs, the temperature of LIBs, and density of LIBs, respectively. Particularly, $\dot{Q}_b$ in Eq. (11) can be calculated by [47]:

$$\dot{Q}_b = Q_{gen}/V_b \tag{13}$$

where Q_{gen} is the generated heat rate of a single battery, and V_b represents the cell's volume. During the discharge operation, the temperature increase is due to reversible and irreversible heat generation. However, as previously discussed, we use a lumped thermal model of LIBs [48]:

$$Q_{gen} = Q_{ir} + Q_{re} = I(U_{OCV} - U) - IT_b \frac{\partial U_{OCV}}{\partial T_b} \tag{14}$$

where Q_{ir} is the irreversible heat generation and Q_{re} is the endothermic reversible heat determined by the discharge process of the LIB. Also, U_{OCV}, I, U, and $\frac{\partial U_{OCV}}{\partial T_{cell}}$ are the open-circuit voltage, discharge current of the battery, batteries' voltage, and the open-circuit voltage's temperature coefficient. According to a previous study [49], throughout the discharge process of the battery pack, it can be concluded that:

$$U = U_{OCV} - IR \tag{15}$$

here, R is the internal resistance which consists of the ohmic and polarization equivalent resistances [50]. Thus, the generated heat rate of LIBs during the discharge operation can be calculated by substituting Eq. (15) into Eq. (14):

$$Q_{gen} = Q_{ir} + Q_{re} = RI^2 - IT_b \frac{\partial U_{OCV}}{\partial T_b} \tag{16}$$

The CuO nanofluid in the indirect cooling channel is modeled using the mixture model, which works based on the single fluid two-phase method. In the mixture method, the velocity vectors of each phase are considered. Hence, volume fractions of each primary and secondary phase within a control volume are used in the following equations:

Continuity equation

$$\nabla \bullet \left(\rho_m u_m\right) = 0 \tag{17}$$

Momentum equation

$$\nabla \bullet \left(\rho_m u_m u_m\right) = -\nabla P_m + \nabla \bullet \left[\tau - \tau_t\right] + \rho_m g + \nabla \bullet \left(\sum_{k=1}^{n} \phi_k \rho_k u_{dr,k} u_{dr,k}\right) \tag{18}$$

Energy equation

$$\nabla \bullet \left(\phi_k u_k (\rho_k h_k + P)\right) = \nabla \bullet \left(K_{eff} \nabla T - C_p \rho_m \overline{ut}\right) \tag{19}$$

Volume fraction equation

$$\nabla \bullet \left(\phi_p \rho_p u_m\right) = -\nabla \bullet \left(\phi_p \rho_p u_{dr,p}\right) \tag{20}$$

$$\rho_m = \sum_{k=1}^{n} \phi_k \rho_k \tag{21}$$

$$\mu_m = \sum_{k=1}^{n} \phi_k \mu_k \tag{22}$$

where μ_m and ρ_m are the mixture's viscosity and density. In Eq. (18), $u_{dr,k}$ is the drift velocity for the secondary phase k, i.e., the nanoparticles in this work.

$$u_{dr,k} = u_k - u_m \tag{23}$$

$$\tau = \mu_m \nabla u_m \tag{24}$$

$$\tau_t = -\sum_{k=1}^{n} \phi_k \rho_k \overline{u_k u_k} \tag{25}$$

2.4. BTMS model

The designed BTMS for this study employs a novel combined indirect/direct liquid cooling system (Fig. 1). The direct liquid-cooled method consists of a simple rectangular cooling channel that immersed all LIBs into the dielectric fluid. In addition, with respect to the indirect cooling approach, four mini-channels are integrated into the batteries' lateral surfaces to improve heat removal, and eventually, the thermal efficiency of the battery pack. The thickness of all cooling channels' walls is selected 2 mm. Fig. 1 illustrates the schematic of the entire BTMS including both indirect and direct cooling channels and separator plates. The dimensions of the direct cooling channel are 206, 707, and 80 mm in width, length, and height, respectively. Additionally, each indirect cooling channel's width, length, and height are 7, 677, and 20 mm, respectively. The indirect and direct cooling channels' hydraulic diameters at the inlet and outlet sections are 5 and 10 mm, respectively. Furthermore, Fig. 2 shows various separator mesh plate configurations. These designs aim to achieve two objectives: firstly, they effectively minimize temperature variations in the LIBs across the direct channel, and secondly, they contribute to reducing the overall temperature of the dielectric coolant as it approaches the outlet section.

In the designed BTMS, the HFE-7100 enters into the direct cooling channel to absorb the generated heat of LIBs through convective heat transfer during the discharge operation at the ambient temperature of 25 °C. During the process of discharging, the heat generated by the first LIBs is transferred to the batteries at the end of the direct channel through the dielectric coolant. Consequently, the temperature of the coolant increases as it flows out of the direct cooling channel, leading to a subsequent rise in the temperature of the batteries near the outlet area. This significantly amplifies the non-uniformity of temperature across the battery pack. Therefore, the batteries have been equipped with four indirect cooling channels positioned both above and below each row of

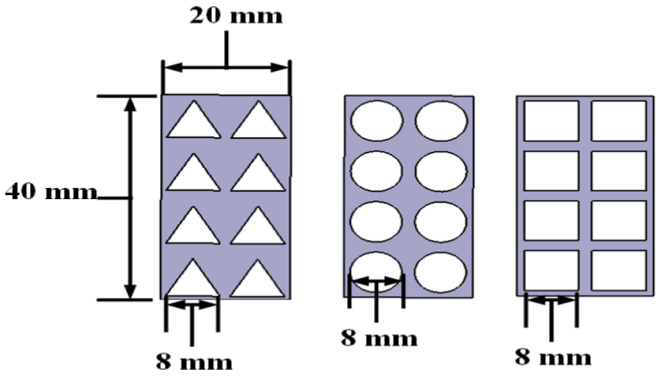

Fig. 2. Schematic of various separator mesh plates.

batteries. This integration ensures that the heat produced and transferred by the LIBs is evenly distributed.

2.4.1. Boundary and initial conditions

In this study, transient numerical simulations are used because batteries undergo a temporary discharge process to analyze the thermal performance of the battery pack. The coolants' initial temperature and ambient temperature are both 25 °C. The inlet and outlet boundary conditions for each cooling channel are constant inflow velocity and static pressure (0 Pa). A no-slip condition is used on all walls. A transient heat source is applied to the LIBs during the discharge process using equations (1–16) implemented by a user-defined function (UDF).

2.4.2. Numerical method

ANSYS-Fluent 19.3 is used for the numerical simulations. Transient simulations are conducted based on the control volume method (CVM) using Eqs. (5–25). The algebraic multigrid-based second-order iterative calculator is employed for the CVM discretization. The SIMPLEC algorithm is used for coupling the velocity and pressure equations. The total computational time depends on the C-rate of batteries during the discharge operation.

The BTMS domain is triangularly meshed (Fig. 3a) and a mesh independence study is performed. Fig. 3(b) illustrates the maximum temperature of the LIB pack during the 1C transient discharge operation for increasing grid numbers. According to the results, the deviations are less than 0.047% from the extrapolated definite values when the grid numbers increase from 6.5×10^5 to 41×10^5. The simulation is continued until the completion of the discharge process at a 1C rate, which requires approximately one hour. Thus, a grid number of 28×10^5 is employed for the next simulations to have efficient performance. In addition, an analysis on the independence of the time step is conducted, which resulted in using a time step of 1.0 s because the obtained results deviate only less than 0.04% from the extrapolated exact values.

3. Results and discussion

A novel cooling system for the new 46800-type Li-ion battery is designed, which includes direct/indirect cooling channels, and meshed separator plates. In this numerical investigation, different influences on the thermal efficiency of the proposed LIB pack are studied, including C-rates (1C, and 3C), direct coolant (dielectric fluid-HFE-7100), indirect coolants (CuO nanofluid and water), mesh plates (circle, square, and triangular), inflow velocity of coolants (0.1–0.3 m/s), inlet/outlet locations, and ambient temperature.

3.1. Validation

To the best of the authors' knowledge, the thermal performance of 46800-type battery pack with a cooling system has not been experimentally studied so far; therefore, the thermal performances of 46800-type battery and liquid cooling system are separately validated. To check the accuracy of the numerical results, a comprehensive validation study has been conducted. First, the lumped thermal model of 46800-format is evaluated and compared with Tranter et al. [51]. They used a coupled electrochemical model and thermal properties for conventional tabbed design to predict the temperature of a 46800-type LIB cell under 1C discharge operation. The computational jelly-roll was formed by rolling a lengthy electrode with two sides upon itself, creating a spiral shape. The battery cell consisted of 40 layers that were rolled, and computational nodes were established at 10-degree intervals within the current collector computational domains, resulting in a resistor model. According to Tranter et al., heat dissipation occurred solely at the outer boundaries of the battery cell [51]. The volumetric heat generation rates of different types of single LIB cells (46800, 21700, and 18650) under 1C discharge operation at the ambient temperature of 25 °C are depicted in Fig. 4(a). The comparison is conducted under the same conditions for the mentioned types of LIBs with NCM cathode. All LIBs feature conventional tab designs and generate heat due to ohmic losses resulting from internal resistances. The calculated heat generation rates in this study align well with the results of Tranter et al. Additionally, it is evident that the heat generation of the 46800-type LIB cell surpasses that of its 18,650 and 21700-type counterparts during 1C discharge operation, highlighting the necessity for highly efficient cooling systems [45,52]. As can be seen in Fig. 4(b), the predicted maximum temperature variations have a good agreement with Tranter et al. [51] a deviation of less than 1.87%. Thus, the lumped thermal model is an excellent choice for the thermal performance evaluation of LIBs even for the new 46800-format batteries.

After validation of the battery thermal model, it is then coupled to the liquid-cooling model. Here, the thermal performance of the cooling system with the battery pack is validated by comparing with the results from our previous experimental study [53], using 21700-type battery equivalents. In the experimental investigation, the thermal behavior of a 21700-format battery pack with 15 cells and an indirect liquid cooling system was reported. In this comparison, water was used to match with experiments. During the 3C discharge operation, the maximum temperature values of the LIB pack were measured using 15 K-type thermocouples positioned at the top section. Initially, the state of charge (SOC) was regulated to 100%. The discharge process was subsequently conducted at an ambient temperature of 25 °C. Based on the experimental findings, the highest temperature in the battery pack was recorded in the last row of cells within the LIB pack. Fig. 4(c) displays the maximum temperature fluctuation of the 21700-type battery pack during the 3C discharge rate, as observed in both experimental and numerical investigations conducted under the same conditions. In addition, we compare the temperature difference of the 21700-type LIB

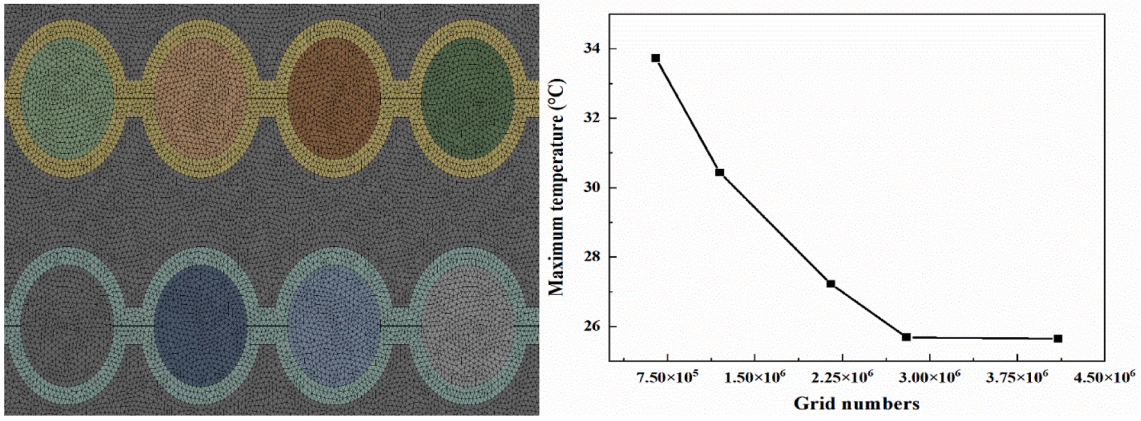

Fig. 3. (a) The meshed BTMS (top view); (b) The variation of the maximum temperature of the LIB pack for various grid numbers.

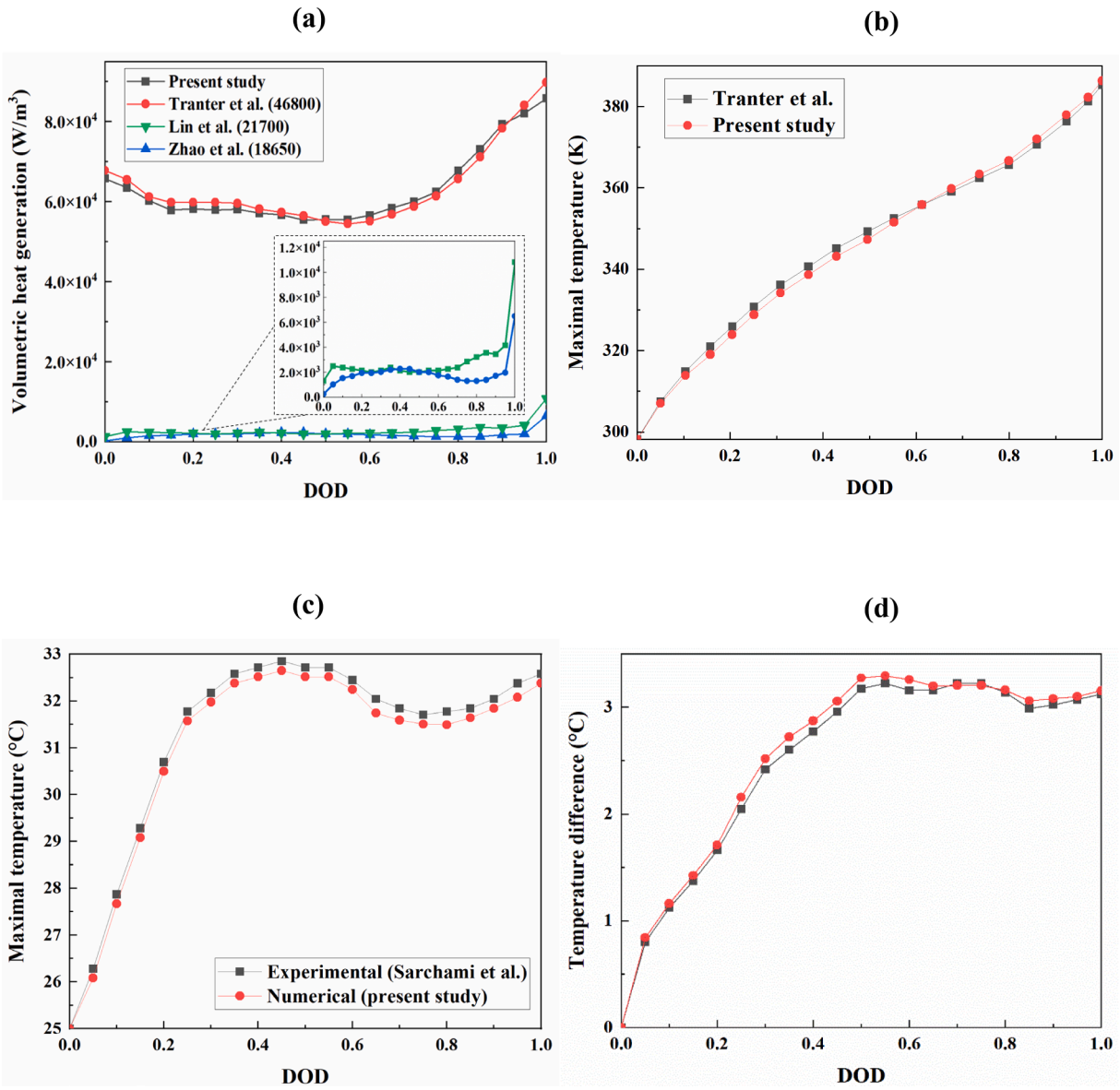

Fig. 4. (a) Heat generation rate comparison of LIB cells vs. DOD; (b) Maximum temperature comparison of 46800-type LIB [51] at 1C discharge; (c and d) Maximum temperature and temperature difference comparison with experimental results [53] for 21700-type LIB pack at 3C discharge.

pack with the experimental results (Fig. 4(d)) in order to highlight the credibility of our computational model. Based on the results of the comparison between the numerical and experimental investigations, the maximum temperature and temperature difference variations of the numerical study has good agreement with the experimental results, with the deviations of less than 3.2% and 6.1%, respectively.

3.2. *Effects of C-rate and coolant*

In this work, the thermal behavior of the battery pack using both indirect and direct liquid-cooled strategies without separator walls is investigated throughout various C-rates (1, and 3), and coolants (water, HFE-7100, and CuO nanofluid). The peak temperature and temperature difference of the battery pack are monitored to fully comprehend what happens inside the LIB pack during different thermal and hydraulic conditions. To evaluate the effects of C-rates and coolants, different combinations of fluids have been used during 1C and 3C discharge operations. Three combinations of coolants including HFE-7100/water, HFE-7100/CuO 2%VF, and HFE-7100/CuO 4%VF are used for direct and indirect cooling channels. The inflow velocities of direct and indirect cooling channels are 0.1 m/s and 0.2 m/s, respectively.

Fig. 5 shows both the maximum temperature (a) and temperature non-homogeneity (b) of the LIB pack during 1C discharge process using different coolants for direct and indirect cooling channels. Based on Fig. 5(a), CuO nanofluid with 2% and 4% volume fractions exhibit lower max temperatures compared to the water in the indirect cooling channels. The maximal temperature values of the LIB pack employing water, 2%, and 4% volume fractions of CuO nanofluids for indirect channels are 31 °C, 29.8 °C, and 28.9 °C, respectively, during the 1C discharge operation. The maximum temperature of the 46800-type battery pack during the 1C discharge process is reduced by 6.7% when 4%VF CuO nanofluid is used instead of water. In addition to the 1C operation, the maximum temperature of the battery pack throughout the 3C discharge process is illustrated in Fig. 6(a) employing similar coolants. It can be observed that the maximum temperature of the LIB pack decreases by 5.2% when a 4% CuO nanofluid is utilized instead of water. The improvements in thermal efficiency of the LIB pack during both 1C and 3C discharge operations can be attributed to the higher thermal conductivity, heat capacity, and ultimately, heat transfer coefficient of the nanofluid. Consequently, the CuO nanofluid exhibits increased

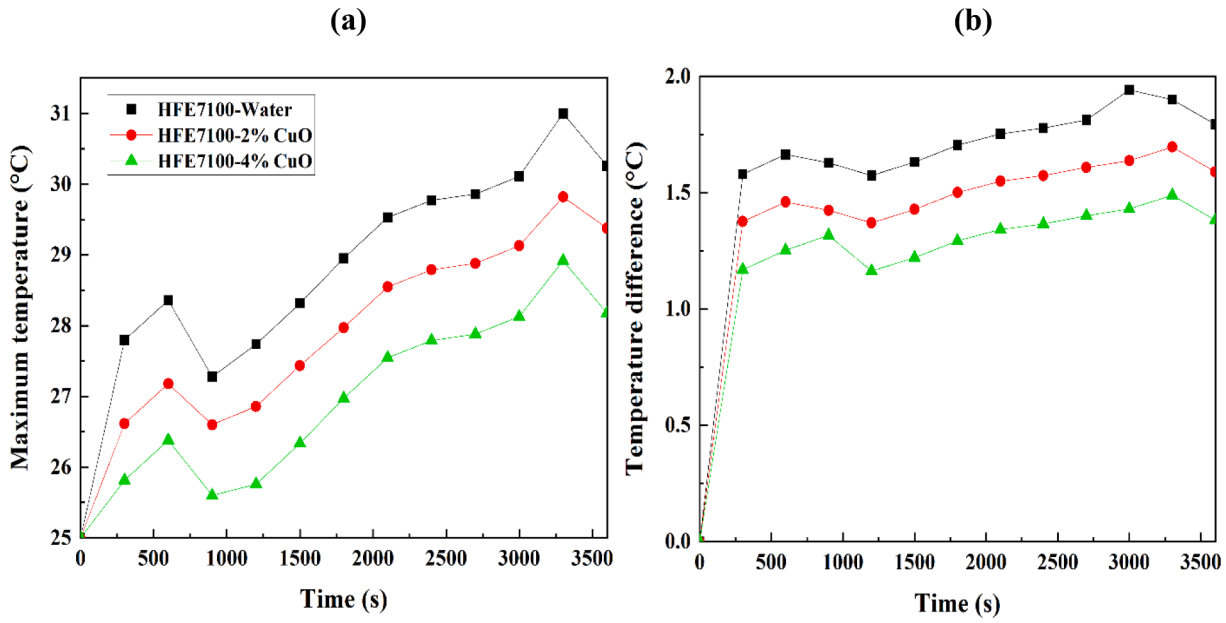

Fig. 5. The temperature variation of 46800-type LIB pack using different coolants during 1C discharge process: (a) peak temperature; (b) temperature difference.

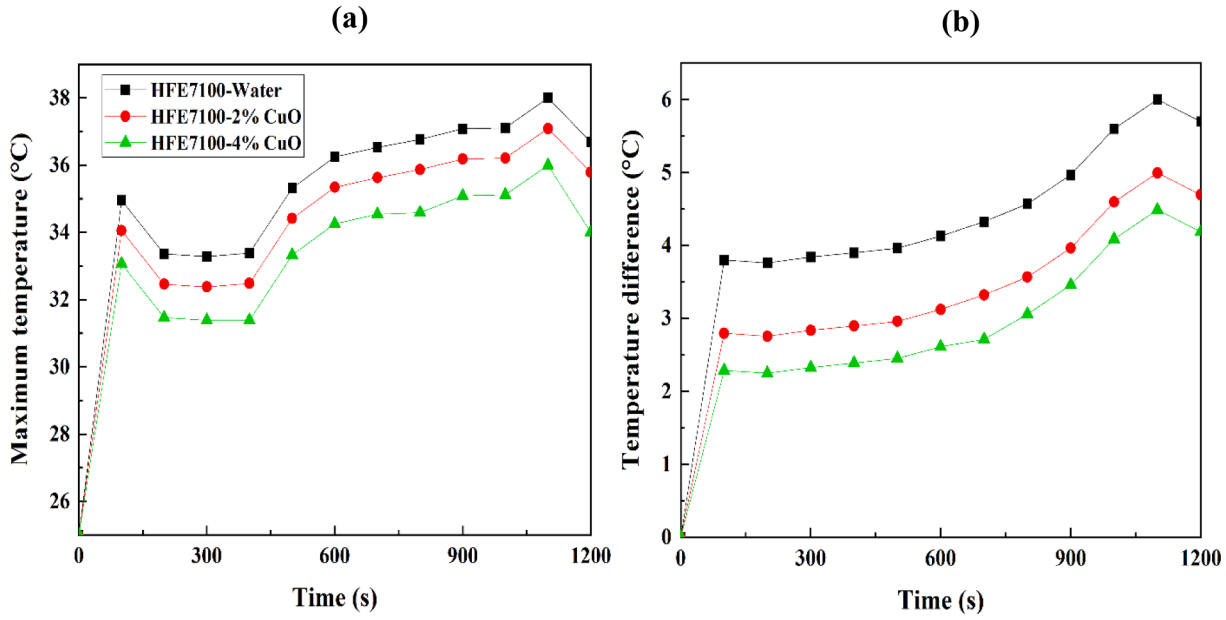

Fig. 6. The temperature variation of 46800-type LIB pack using different coolants during 3C discharge process: (a) peak temperature; (b) temperature difference.

convective heat transfer, which reduces the temperature of LIBs. As expected, a higher volume fraction favorably affects the thermal efficiency of the battery pack during the operation.

Fig. 5(b) and Fig. 6(b) exhibit that the temperature non-homogeneities of the battery pack notably improved by using the CuO nanofluids in indirect cooling channels. The results show that temperature differences of LIB pack throughout 1C and 3C discharge processes reduced by 0.46 °C, and 1.52 °C, respectively, when indirect channels employed 4% CuO nanofluid instead of water. Throughout 1C and 3C discharge operations, the temperature variations of LIBs are directly dependent on the heat generation rates of cells.

Based on the temperature difference illustrated in Figs. 5 and 6, the improvement percentages for 1C and 3C processes are 23.5% and 28%, respectively, when comparing different combinations of coolants. From these results, we can infer that the main contributing factor to the limited improvement observed in the 1C process, in comparison to the 3C process, is the lower heat generation rates of LIBs during the 1C process. These lower heat rates did not negatively affect the thermal condition of the battery pack. Hence, we can conclude that water, as a coolant, can effectively manage the thermal efficiency of the battery pack during 1C discharge operations. However, for high C-rates (fast discharging), it is recommended to use CuO nanofluid to handle the maximum temperature and temperature non-homogeneity of the battery pack.

The peak temperature and temperature difference of the LIB pack suddenly increase during the initial stages. Following the sudden increase, a temperature drop occurred, influenced by two factors: the direct impact of LIB heat generation rates on temperature variations in LIBs, which decreased due to variations in local current density [51], and the initial efficacy of the highly efficient proposed cooling system in

reducing temperature. After a short thermal equilibrium between generated heat of LIBs and the heat removal of coolants; again, temperature values increased during the final stages of the process. Essentially, Figs. 5 and 6 indicate that the peak temperature and temperature difference of LIBs during 3C discharge process are significantly increased by 17.1% and 66.9%, respectively, compared to 1C process even with using 4%VF CuO nanofluid. The most cogent reason for worsening the thermal behavior of the battery pack during high C-rates is that a high voltage drop happens inside the LIBs while the current rate is increased. Due to this phenomenon, the cutoff voltage reaches a lower SOC in the cathode; thus, causing a higher SOC in the anode [54]. Consequently, the heat generation rate of 46800-type Li-ion batteries is increased.

Accordingly, the thermal behavior of LIBs indicated that the CuO nanofluid with any volume fraction in the proposed cooling system is sufficient for low C-rate (less than1C) discharge processes. However, C-rates > 1 produce higher heat inside the LIBs requiring high efficiency BTMS. The following sub-sections provide more practical and effective strategies to upgrade the combined direct/indirect liquid-cooled system.

3.3. Effect of using meshed separator plates

In this sub-section, the influence of employing separator plates with different types of mesh on the thermal behavior of 46800-format battery pack is evaluated throughout the 3C discharge operation. According to the outcomes of the previous sub-section, the proposed cooling system is not acceptable due to the high temperature variations during 3C discharge process. Hence, mesh separator plates are added to increase overall convective heat transfer and lower LIB temperature peaks. HFE-7100 and 4%-VF CuO nanofluid are chosen for direct and indirect cooling channels, respectively; also, the inflow velocities are 0.1 m/s and 0.2 m/s for direct and indirect channels. Through this evaluation, different arrangements for BTMS with and without separator plates are considered to assess the highest temperature and temperature difference of the battery pack. As can be seen in Fig. 2, various shapes of meshed separator plates are designed including simple, circular, square, and triangular.

The LIB pack's peak temperature and temperature non-uniformity for various cases are depicted in Fig. 7. Clearly, the circular case has the most effect on reducing the maximal temperature of the LIB pack, followed by the square, triangular, simple, and no-wall. The maximal temperature decreased by 10.5% when the cooling system used circular mesh walls compared to the no-wall case. Similarly, as illustrated in Fig. 7(b), the thermal performance of the LIB pack is improved by 22.7% by using the circular case in comparison to the no-wall case. Based on the outcome of this section, the thermal behavior of the battery pack is enhanced by employing each type of mesh plate. Therefore, using meshed separator walls should be taken into account for LIB packs in electric vehicles. One of the main reasons for employing mesh plates is to fully exploit the coolant's capabilities in the direct cooling channel. Previously, coolant would enter the channel through the inlet and immediately exit through the outlet, causing numerous issues, such as thermal non-uniformity [53]. This rapid discharge of coolant resulted in diminished cooling capacity within the channel, undeveloped thermal and hydraulic flow, and increased thermal non-uniformity for LIBs. Additionally, the presence of low-flow areas among LIBs led to the formation of hot spots. This issue can be addressed by incorporating separator mesh plates to promote turbulent flow through the mixing effect and enhance heat transfer as HFE-7100 flows into the direct channel towards the outlet section. Therefore, by comparing various common shapes, we are able to optimize the thermal performance of the LIB pack.

The most significant impact of the meshed separator plates is on the temperature variation in the battery pack. This is highlighted in 2D top view contours to depict the thermal behavior of the battery pack during high heat generation rates of LIBs. Four different cases, namely no-wall, simple, circular, and triangular are exhibited in Fig. 8. Comparing the simple wall case with other meshed plates, the core temperature of LIBs notably reduced when the mesh plates are added. The circular plate has the best thermal performance compared to other geometries tested.

Thus, in the high C-rates cases where temperature variation is a critical concern, meshed separator plates are recommended. These proposed structures can be useful in regulating temperature differences in the LIB pack.

3.4. Effect of indirect/direct inflow velocity

The influence of the indirect and direct inflow velocities on the thermal performance of the LIB pack throughout the 3C discharge operation has also been evaluated. To comprehensively assess the effect of flow rate in both types of channels, different inflow velocities for HFE-7100 in the direct channel (0.1, 0.15, and 0.2 m/s), and 4% CuO

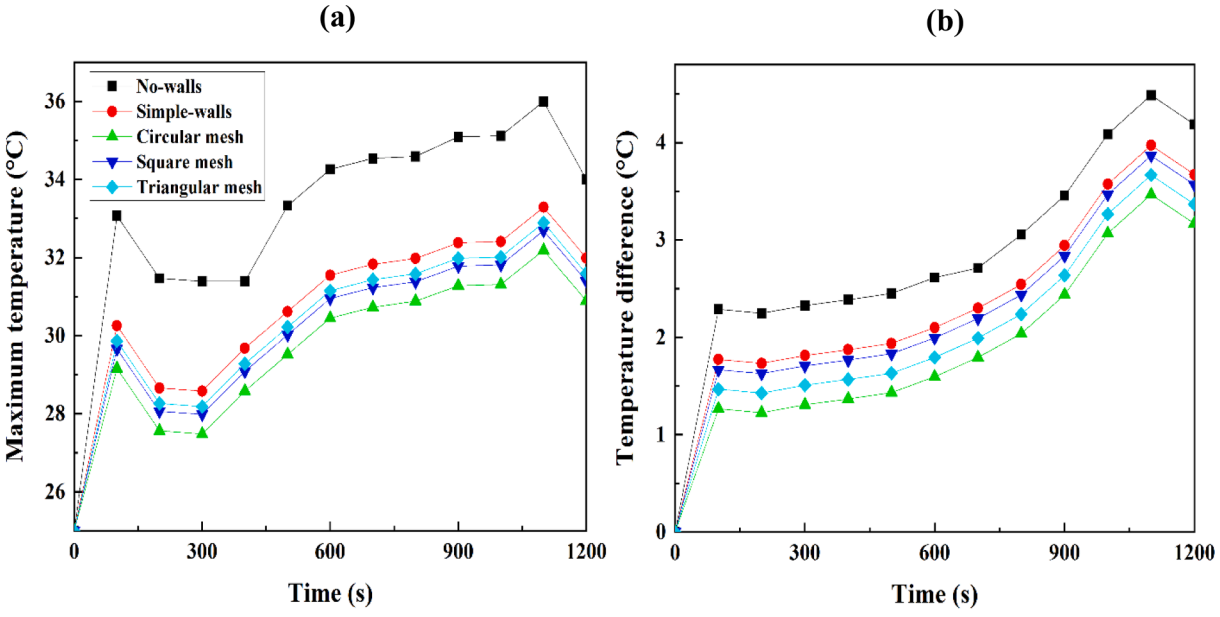

Fig. 7. The temperature variation of 46800-type LIB pack using various meshed separator plates: (a) peak temperature; (b) temperature difference.

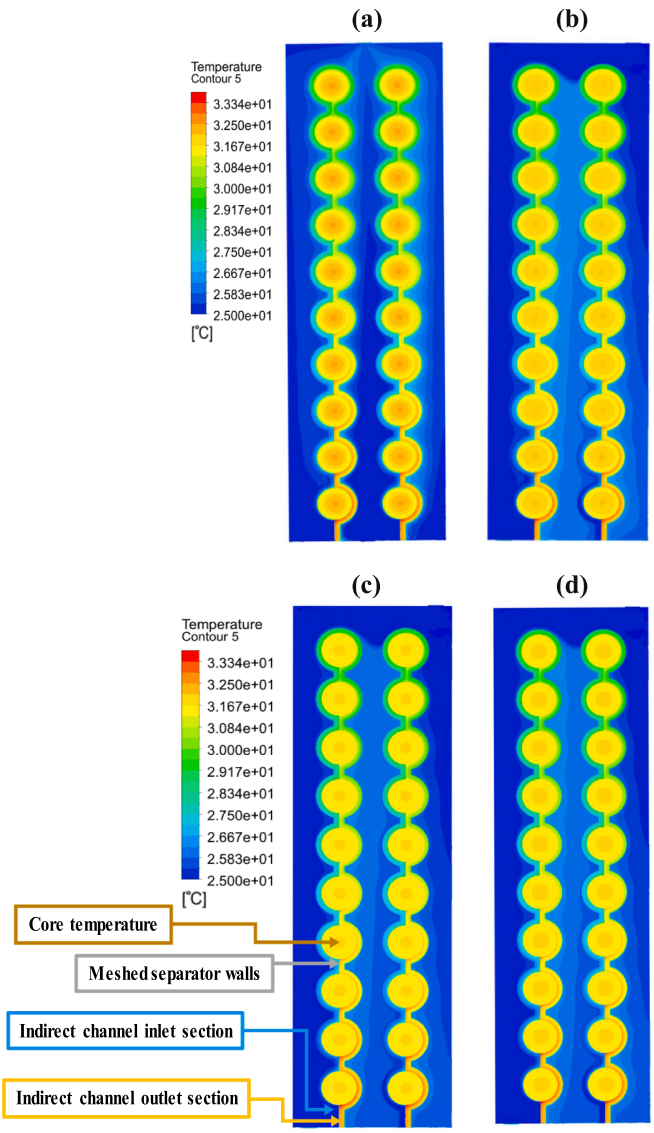

Fig. 8. The 2D top view contours of the battery pack's temperature variation employing different meshed separator walls: (a) No-walls; (b) Simple; (c) Circular; (d) Triangular.

nanofluid in the indirect channel (0.2, 0.25, and 0.3 m/s) are considered. Based on the results from the previous section, the circular meshed separator walls are integrated into the direct cooling channel for maximum thermal performance during the high C-rate process. It should be noted that the present work did not consider the immersion cooling method which coolant does not move in the direct cooling channel and the flow cooling method is used for all simulations due to its high thermal reliability. However, immersion cooling performance can be readily obtained by evaluating the limit where inlet velocity → zero.

Fig. 9 depicts the highest temperature and temperature variation observed in the battery pack across different scenarios. There are three scenarios that include the combinations of inflow velocities. The first case is the combination of 0.2 and 0.1 m/s velocities for indirect and direct channels, respectively. The second and third cases' combinations of velocities are 0.25/0.15 m/s, and 0.3/0.2 m/s, respectively, for indirect and direct channels. As seen in Fig. 9(a), the peak temperature of the battery pack decreases from 32.19 °C to 30.8 °C when the inflow velocities of the indirect and direct channels are increased from 0.2 to 0.3 m/s and from 0.1 to 0.2 m/s, respectively. This maximal temperature reduction improved the thermal performance of the battery pack by 4.3%. Furthermore, by increasing the inflow velocities of the cooling channels, Fig. 9(b) demonstrates a notable reduction in the temperature non-homogeneity of the battery pack throughout its operation. For instance, the temperature difference of the LIB pack is reduced from 3.47 °C to 3.06 °C while the inflow velocities of the indirect and direct channels increased from 0.1 to 0.2 m/s, and from 0.2 to 0.3 m/s, respectively. The thermal behavior of the battery pack is enhanced by 11.8% when both indirect and direct cooling channels used high inflow velocities (0.2 and 0.3 m/s). Increasing the inflow velocity of the cooling channels not only increases the momentum of the coolants in the channel but also increases the heat transfer of both direct and indirect liquid cooling systems. Therefore, by increasing the heat transfer during the operation, the peak temperature and temperature non-uniformity of the battery pack is correspondingly reduced.

According to Fig. 10, the temperature contours of the cooling systems with LIBs are illustrated for cases 1 and 3 at the end of the discharge operation. As indicated, the batteries located in case 1, especially in the first columns, have a higher core temperature. This is due to the higher inflow velocity of case 3 compared to case 1. Additionally, it can be observed that the temperature of the indirect cooling channels monotonically increases as the nanofluid circulates around the LIBs towards the outlet section, and this effect is more pronounced in case 1. This is anticipated since the coolant temperature increases as it absorbs the generated heat of the LIBs towards the outlet.

3.5. Effect of coolant flow direction

While increasing the inflow velocities of both direct and indirect cooling channels enhances the thermal efficiency of the battery pack, this improvement may come at the expense of increased pressure drop within the cooling channels, resulting in higher pumping power requirements. Based on the previous sub-section's outcome, case 3 has the best performance; but, a higher overall power might be consumed. Therefore, in this subsection, we examine a practical approach to predicting the impact of the inlet and outlet positions in the direct cooling channel on thermal efficiency. To improve the thermal behavior of the LIB pack, the inlet/outlet locations are changed from both the left side of the channel to the inlet-left and outlet-right locations. Different inflow velocities for these two locations are used to comprehensively evaluate the effect of the fluid flow direction in the direct cooling channel. Other thermal and hydraulic conditions of the BTMS are similar to the previous section.

The peak temperature and temperature diversity of the LIB pack for various locations of the inlet and outlet are shown in Fig. 11(a) and (b), respectively. The results show that using the inlet-left side and outlet-right side of the direct cooling channel reduces the maximal temperature of the LIB even with lower inflow velocity (case 1) compared to both left-side inlet/outlet. The maximal temperature of case 3 with left-inlet/right-outlet is decreased by 1.2 °C compared to case 3 with both left inlet/outlet. This reduction of the maximal temperature leads to a 3.8% improvement in the thermal performance of the battery pack. The principal reason for this improvement is the proper temperature uniformity of LIBs by changing the coolant flow direction in the direct cooling channel. The temperature non-homogeneity of the LIB pack is also reduced from 3.06 °C to 2.68 °C by using left-inlet/right-outlet locations of the channel compared to both left-side locations. Moreover, the LIB pack with lower inflow velocity (case 1) and the new flow direction (In-left/Out-right) has better thermal performance (6.5%) compared to the higher velocity (case 3) without changing the flow direction.

3.6. Effect of ambient temperature

The impact of different ambient temperatures on the performance of the proposed cooling system is assessed to analyze its effectiveness in various weather conditions. In addition to the 25 °C ambient

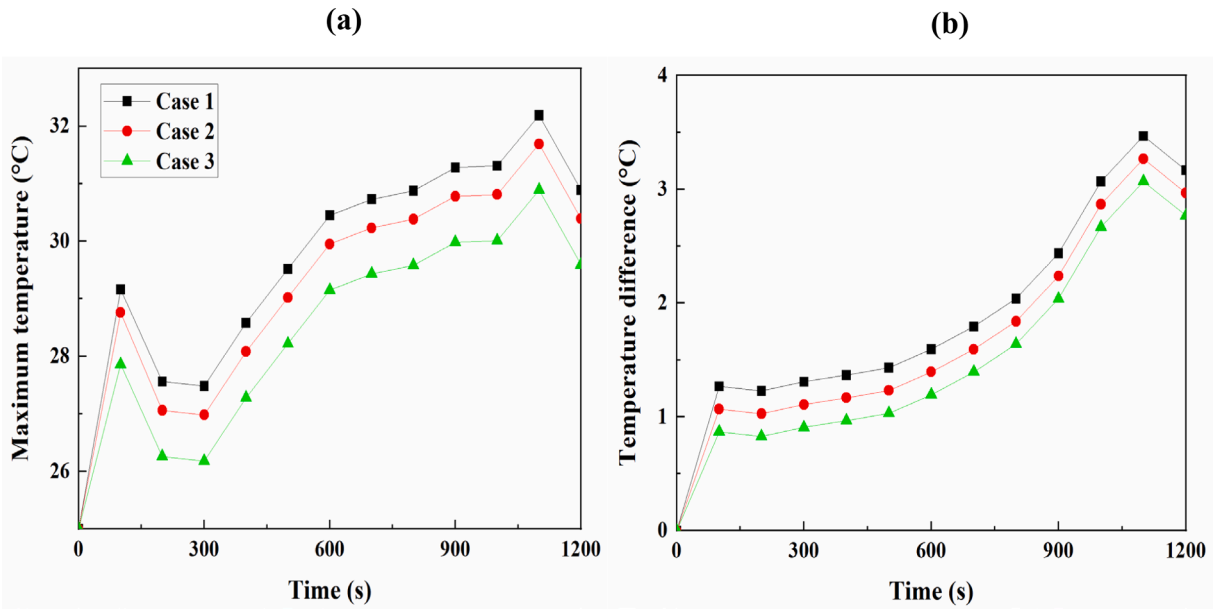

Fig. 9. The temperature variation of 46800-type LIB pack using different combinations of inflow velocities; case 1: 0.2/0.1 m/s, case 2: 0.25/0.15 m/s, and case 3: 0.3/0.2 m/s are the for indirect and direct channels, respectively; (a) peak temperature; (b) temperature difference.

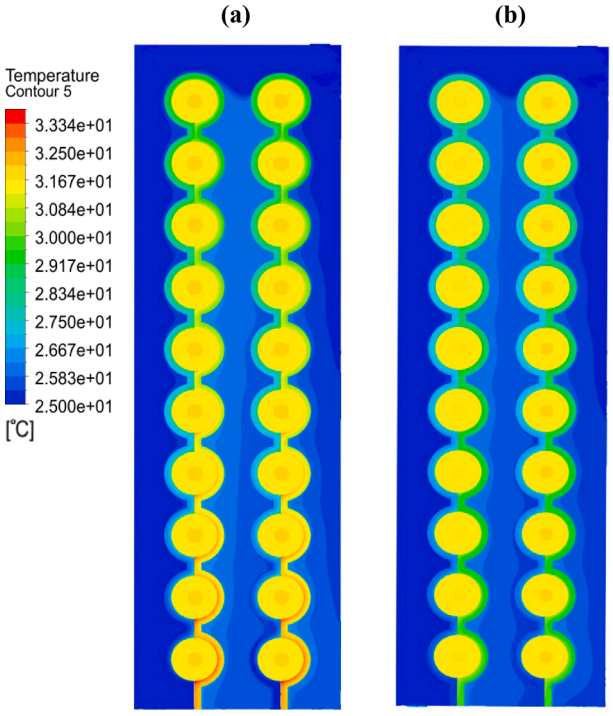

Fig. 10. The 2D top view temperature contours of the battery pack: (a) case 1; (b) case 3.

temperature utilized in previous sections, three additional temperatures are considered: 30 °C, 35 °C, and 40 °C. Based on previous findings, the optimal parameters for the cooling system as discussed in previous sections areemployed. It is important to note that all solid components, such as the LIBs and cooling channels, initially start at 25 °C but change once the discharge operation commences. For example, when the ambient temperature is set to 40 °C, all solid components begin with an initial temperature of 25 °C. In addition, coolants enter the channels at a consistent 25 °C temperature for all cases. This approach enables an examination of how ambient temperature affects the thermal performance of the LIB pack in an electric vehicle during different weather conditions [55].

Fig. 12 illustrates the peak temperature and temperature difference of the LIB pack under 3C rate discharge processes, considering various ambient temperatures. In Fig. 12(a), the maximum temperature curves for different ambient temperatures initially began at 25 °C, but the gaps between them noticeably increased towards the end of the operation. While the temperature intervals between the maximum temperature curves remained around 2 °C during the initial periods of the discharge process, after approximately 10 min of operation, the gaps gradually expanded, reaching 6.7 °C between the 35 °C and 40 °C curves. Additionally, it is evident that the maximum temperature of the LIB pack exceeded the safe limit of 25 °C – 40 °C when the ambient temperature was 40 °C. This variation primarily results from the influence of ambient temperature, which significantly affects the maximum temperature of the LIB pack. Consequently, this increase indicates that the cooling system becomes more vulnerable as the ambient temperature rises. Similarly, Fig. 12(b) displays the temperature difference of the LIB pack, following a similar pattern observed in the maximum temperature curves. In conclusion, even with a consistent coolant inlet temperature of 25 °C, effectively controlling and managing the high heat generation rate of the 46800-type LIB pack at an ambient temperature of 40 °C becomes challenging. Therefore, it can be inferred that high ambient temperatures, such as 40 °C, have an adverse effect on the thermal performance of the LIB pack, even when utilizing an optimized combined liquid cooling system. However, the proposed cooling system can stabilize the maximum temperature and temperature difference of the LIB pack during the discharge operation at ambient temperatures of 30 °C and 35 °C.

3.7. Pressure drop

After the comparative studies of using 2% and 4% CuO nanofluids with different inflow velocities, the pressure drop evaluation in both direct and indirect cooling channels should be taken into account. Moreover, since the LIB pack provides the required energy for pumping the coolants into the channels, it is of importance to analyze the pressure drop values in detail. It should be noted that the flow rate and nanofluid's volume fraction have a direct relation to the pressure drop and correspondingly to the pumping power as well. The pressure drop

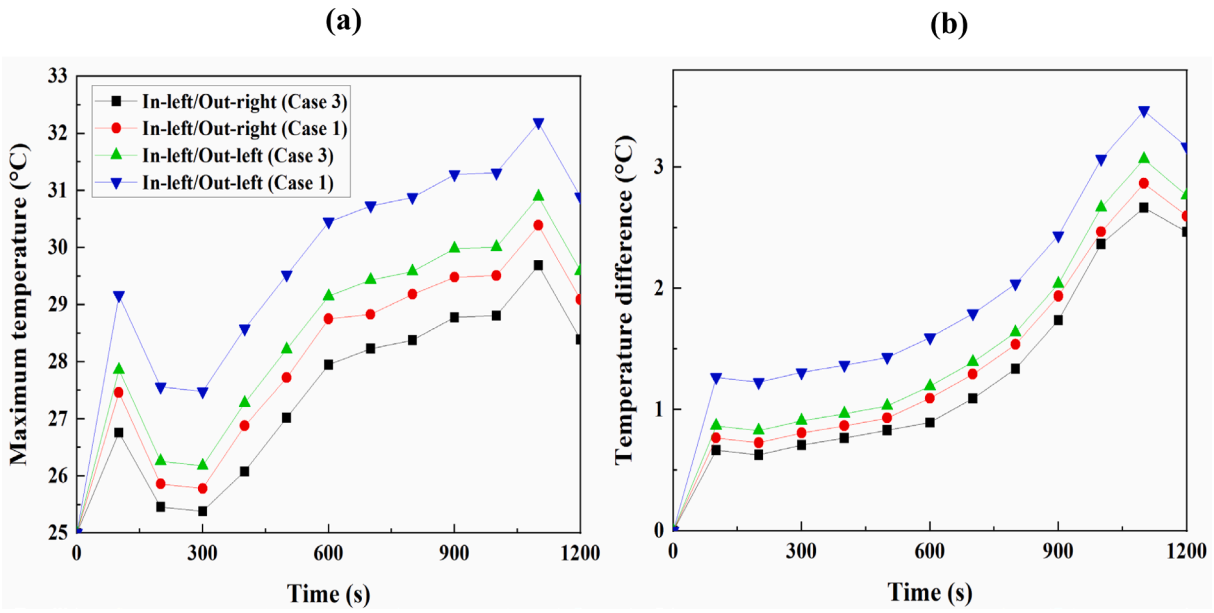

Fig. 11. The temperature variation of 46800-type LIB pack using different inlet/outlet locations, case 1: 0.2 m/s (indirect)/0.1 m/s (direct), and case 3: 0.3 m/s (indirect)/0.2 m/s (direct): (a) peak temperature; (b) temperature difference.

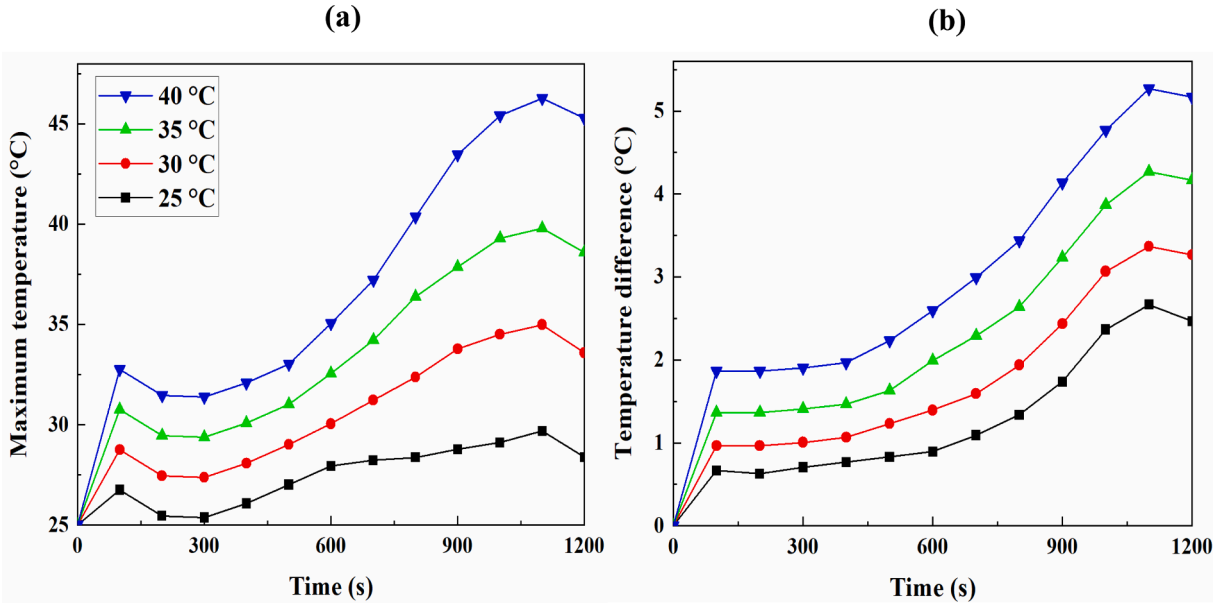

Fig. 12. The temperature variation of 46800-type LIB pack at different ambient temperatures: (a) peak temperature; (b) temperature difference.

variations of the direct and one of the indirect channels are indicated in Fig. 13(a) and (b), respectively. As illustrated, increasing the Reynolds number of the coolants, and the nanofluid's volume fraction caused the increment of pressure drop value. For instance, the pressure drop in the direct channel increased by 59.5% when the Reynolds number increased from 2475.4 to 4950.8. Also, the pressure drop of 4%-VF CuO nanofluid is increased by 55% compared to the water in the indirect channel at an inflow velocity of 0.3 m/s.

4. Conclusions

This study utilizes an innovative approach of combined direct and indirect liquid cooling to improve the thermal efficiency of a newly developed 46800-type LIB pack. The novel design incorporates HFE-7100 (direct cooling) and CuO nanofluid (indirect cooling) channels and a mesh separator plate to prevent flow bypass and enhance mixing. The thermal performance of the battery pack is assessed under different conditions and the maximum temperature and temperature difference within the pack are reported. The following conclusions can be reached from the results:

- The results indicated that using a 4%-VF CuO nanofluid in the indirect channels resulted in a 25% improvement in the thermal performance of LIBs, specifically in terms of temperature uniformity, during a 3C discharge operation, as compared to water.
- Due to the loss of voltage in LIBs under 3C-rate operation, more heat is generated in the LIBs, which worsened the thermal efficiency by 66.9% compared to 1C operation.
- After achieving high temperature variations in the battery pack during 3C discharge process, novel meshed separator plates with

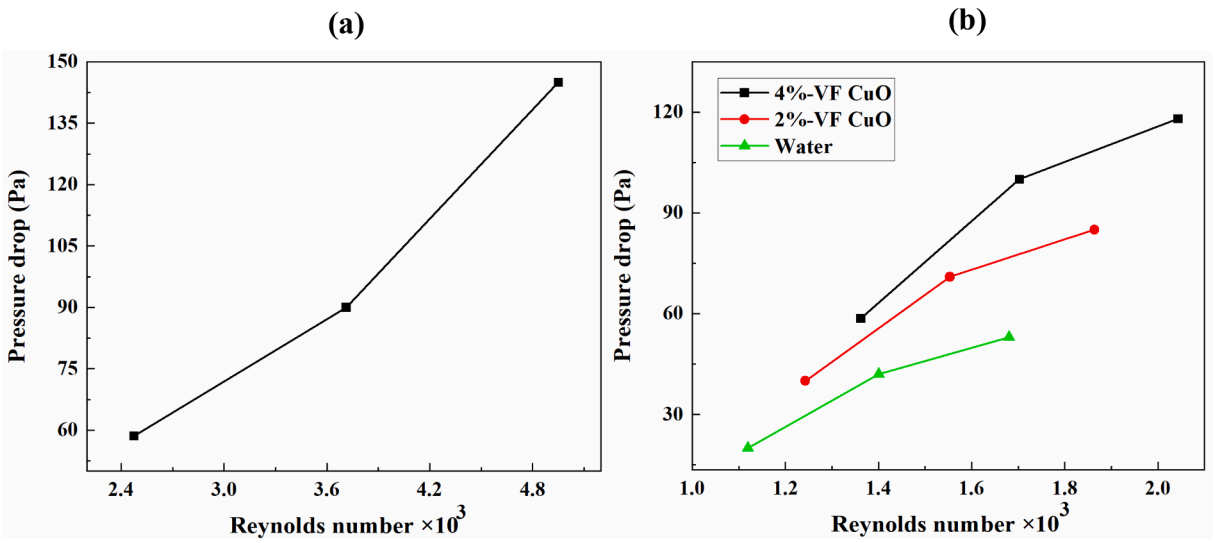

Fig. 13. The pressure drop variation of direct and indirect cooling channels for various Reynolds numbers (a) direct cooling channel; (b) indirect cooling channel.

different shapes (circular, square, triangular, and simple) are designed for the direct cooling channel. The LIB pack that used circular meshed separator plates demonstrated a decrease of 3.81 °C in peak temperature and a 1 °C reduction in temperature difference when compared to the configuration that did not have a mesh separator plate. The temperature contours reveal that incorporating circular meshed separator walls enhanced the temperature uniformity of the LIB pack by 22.7%.

- Moreover, when utilizing inflow velocities of 0.2 m/s and 0.3 m/s (case 3) for the indirect and direct channels, respectively, the maximum temperature of LIBs is reduced by 1.3 °C in comparison to using inflow velocities of 0.1 m/s and 0.2 m/s (case 1).
- A new technique has been introduced to address the impact of rising pressure drop resulting from an increase in flow rate within the liquid cooling channels. This technique involves modifying the inlet and outlet sections of the direct cooling channel to optimize the thermal performance of the battery pack. By implementing this approach, the thermal performance of the LIB pack in Case 1, using the left-inlet/right-outlet configuration, demonstrates a 6.5% improvement compared to Case 3, which employs the left-inlet/left-outlet sections. These results highlight the significance of flow direction within the cooling channel, even when working at a low flow rate.
- The performance of the proposed cooling system is analyzed at different ambient temperatures (25 °C, 30 °C, 35 °C, and 40 °C) to evaluate its effectiveness under various weather conditions. At an ambient temperature of 40 °C, the maximum temperature of the LIB pack reached 45.2 °C, which exceeded the acceptable range. However, with the optimized cooling system operating at 35 °C, the maximum temperature (38.5 °C) and temperature difference (4.1 °C) were maintained within desirable ranges

Declaration of Competing Interest

The authors declare that they have no known competing financial interests or personal relationships that could have appeared to influence the work reported in this paper.

Data availability

Data will be made available on request.

References

[1] A. Sajjad, F. Asmi, J. Chu, M.A. Anwar, Environmental concerns and switching toward electric vehicles: Geographic and institutional perspectives, Environ. Sci. Pollut. Res. 27 (2020) 39774–39785, https://doi.org/10.1007/s11356-020-08311-4.
[2] F. Zhang, X. Hu, R. Langari, D. Cao, Energy management strategies of connected HEVs and PHEVs: Recent progress and outlook, Prog. Energy Combust. Sci. 73 (2019) 235–256, https://doi.org/10.1016/j.pecs.2019.04.002.
[3] Z. Cabrane, D. Batool, J. Kim, K. Yoo, Design and simulation studies of battery-supercapacitor hybrid energy storage system for improved performances of traction system of solar vehicle, J. Storage Mater. 32 (2020) 101943, https://doi.org/10.1016/j.est.2021.102454.
[4] P. Ahmadi, S.H. Torabi, H. Afsaneh, Y. Sadegheih, H. Ganjehsarabi, M. Ashjaee, The effects of driving patterns and PEM fuel cell degradation on the lifecycle assessment of hydrogen fuel cell vehicles, Int. J. Hydrogen Energy 45 (2020) 3595–3608, https://doi.org/10.1016/j.ijhydene.2019.01.165.
[5] R.R. Kumar, K. Alok, Adoption of electric vehicle: A literature review and prospects for sustainability, J. Clean. Prod. 253 (2020) 119911, https://doi.org/10.1016/j.jclepro.2019.119911.
[6] X. Lai, Q. Chen, X. Tang, Y. Zhou, F. Gao, Y. Guo, R. Bhagat, Y. Zheng, Critical review of life cycle assessment of lithium-ion batteries for electric vehicles: A lifespan perspective, eTransportation (2022) 100169, https://doi.org/10.1016/j.etran.2022.100169.
[7] J. Liang, Y. Gan, Y. Li, M. Tan, J. Wang, Thermal and electrochemical performance of a serially connected battery module using a heat pipe-based thermal management system under different coolant temperatures, Energy 189 (2019) 116233, https://doi.org/10.1016/j.energy.2019.116233.
[8] L.H. Saw, Y. Ye, A.A. Tay, Integration issues of lithium-ion battery into electric vehicles battery pack, J. Clean. Prod. 113 (2016) 1032–1045, https://doi.org/10.1016/j.jclepro.2015.11.011.
[9] X. Feng, S. Zheng, D. Ren, X. He, L. Wang, H. Cui, X. Liu, C. Jin, F. Zhang, C. Xu, Investigating the thermal runaway mechanisms of lithium-ion batteries based on thermal analysis database, Appl. Energy 246 (2019) 53–64, https://doi.org/10.1016/j.apenergy.2019.04.009.
[10] J. Liang, Y. Gan, M. Yao, Y. Li, Numerical analysis of capacity fading for a LiFePO4 battery under different current rates and ambient temperatures, Int. J. Heat Mass Transf. 165 (2021) 120615, https://doi.org/10.1016/j.ijheatmasstransfer.2020.120615.
[11] N. Piao, X. Gao, H. Yang, Z. Guo, G. Hu, H.-M. Cheng, F. Li, Challenges and development of lithium-ion batteries for low temperature environments, eTransportation 11 (2022) 100145, https://doi.org/10.1016/j.etran.2021.100145.
[12] M. Tan, Y. Gan, J. Liang, L. He, Y. Li, S. Song, Y. Shi, Effect of initial temperature on electrochemical and thermal characteristics of a lithium-ion battery during charging process, Appl. Therm. Eng. 177 (2020) 115500, https://doi.org/10.1016/j.applthermaleng.2020.115500.
[13] A. Sarchami, M. Najafi, A. Imam, E. Houshfar, Experimental study of thermal management system for cylindrical Li-ion battery pack based on nanofluid cooling and copper sheath, Int. J. Therm. Sci. 171 (2022) 107244, https://doi.org/10.1016/j.ijthermalsci.2021.107244.
[14] L. Sheng, H. Zhang, L. Su, Z. Zhang, H. Zhang, K. Li, Y. Fang, W. Ye, Effect analysis on thermal profile management of a cylindrical lithium-ion battery utilizing a cellular liquid cooling jacket, Energy 220 (2021) 119725, https://doi.org/10.1016/j.energy.2020.119725.
[15] P. Peng, Y. Wang, F. Jiang, Numerical study of PCM thermal behavior of a novel PCM-heat pipe combined system for Li-ion battery thermal management, Appl.

Therm. Eng. 209 (2022) 118293, https://doi.org/10.1016/j.applthermaleng.2022.118293.
[16] M.M. El Idi, M. Karkri, M.A. Tankari, A passive thermal management system of Li-ion batteries using PCM composites: Experimental and numerical investigations, Int. J. Heat Mass Transf. 169 (2021) 120894, https://doi.org/10.1016/j.ijheatmasstransfer.2020.120894.
[17] Y. Gan, J. Wang, J. Liang, Z. Huang, M. Hu, Development of thermal equivalent circuit model of heat pipe-based thermal management system for a battery module with cylindrical cells, Appl. Therm. Eng. 164 (2020) 114523, https://doi.org/10.1016/j.applthermaleng.2019.114523.
[18] J. Wang, Y. Gan, J. Liang, M. Tan, Y. Li, Sensitivity analysis of factors influencing a heat pipe-based thermal management system for a battery module with cylindrical cells, Appl. Therm. Eng. 151 (2019) 475–485, https://doi.org/10.1016/j.applthermaleng.2019.02.036.
[19] Q. Yue, C. He, M. Wu, T. Zhao, Advances in thermal management systems for next-generation power batteries, International Journal of Heat and Mass Transfer 181 (2021) 121853, https://doi.org/10.1016/j.ijheatmasstransfer.2021.121853.
[20] A.K. Thakur, R. Sathyamurthy, R. Velraj, R. Saidur, A. Pandey, Z. Ma, P. Singh, S. K. Hazra, S.W. Sharshir, R. Prabakaran, A state-of-the art review on advancing battery thermal management systems for fast-charging, Appl. Therm. Eng. 226 (2023) 120303, https://doi.org/10.1016/j.applthermaleng.2023.120303.
[21] W.P. Harris, U. Ashraf, R.W. Thibault, N. Certo, P. Dubey, K. Galvan, Cold plate blade for battery modules, in, Google Patents, 2023.
[22] G. Pulugundla, P. Dubey, A. Srouji, Time-accurate CFD analysis of liquid cold plates for efficient thermal performance of electric vehicle Li-ion battery modules, in, SAE Technical Paper, 2019.
[23] A. Sarchami, M. Tousi, M. Kiani, A. Arshadi, M. Najafi, M. Darab, E. Houshfar, A novel nanofluid cooling system for modular lithium-ion battery thermal management based on wavy/stair channels, Int. J. Therm. Sci. 182 (2022) 107823, https://doi.org/10.1016/j.ijthermalsci.2022.107823.
[24] H. Liu, X. Gao, J. Zhao, M. Yu, D. Niu, Y. Ji, Liquid-based battery thermal management system performance improvement with intersected serpentine channels, Renew. Energy 199 (2022) 640–652, https://doi.org/10.1016/j.renene.2022.09.026.
[25] M. Tousi, A. Sarchami, M. Kiani, M. Najafi, E. Houshfar, Numerical study of novel liquid-cooled thermal management system for cylindrical Li-ion battery packs under high discharge rate based on AgO nanofluid and copper sheath, J. Storage Mater. 41 (2021) 102910, https://doi.org/10.1016/j.est.2021.102910.
[26] C. Roe, X. Feng, G. White, R. Li, H. Wang, X. Rui, C. Li, F. Zhang, V. Null, M. Parkes, Immersion cooling for lithium-ion batteries–A review, J. Power Sources 525 (2022) 231094, https://doi.org/10.1016/j.jpowsour.2022.231094.
[27] Y.-F. Wang, J.-T. Wu, Thermal performance predictions for an HFE-7000 direct flow boiling cooled battery thermal management system for electric vehicles, Energ. Conver. Manage. 207 (2020) 112569, https://doi.org/10.1016/j.enconman.2020.112569.
[28] S. Wu, L. Lao, L. Wu, L. Liu, C. Lin, Q. Zhang, Effect analysis on integration efficiency and safety performance of a battery thermal management system based on direct contact liquid cooling, Appl. Therm. Eng. 201 (2022) 117788, https://doi.org/10.1016/j.applthermaleng.2021.117788.
[29] S.H. Hong, D.S. Jang, S. Park, S. Yun, Y. Kim, Thermal performance of direct two-phase refrigerant cooling for lithium-ion batteries in electric vehicles, Appl. Therm. Eng. 173 (2020) 115213, https://doi.org/10.1016/j.applthermaleng.2020.115213.
[30] P. Dubey, G. Pulugundla, A. Srouji, Direct comparison of immersion and cold-plate based cooling for automotive Li-ion battery modules, Energies 14 (2021) 1259, https://doi.org/10.3390/en14051259.
[31] M. Kiani, S. Omiddezyani, A.M. Nejad, M. Ashjaee, E. Houshfar, Novel hybrid thermal management for Li-ion batteries with nanofluid cooling in the presence of alternating magnetic field: An experimental study, Case Studies in Thermal Engineering 28 (2021) 101539, https://doi.org/10.1016/j.csite.2021.101539.
[32] M. Mashayekhi, E. Houshfar, M. Ashjaee, Development of hybrid cooling method with PCM and Al2O3 nanofluid in aluminium minichannels using heat source model of Li-ion batteries, Appl. Therm. Eng. 178 (2020) 115543, https://doi.org/10.1016/j.applthermaleng.2020.115543.
[33] M. Kiani, S. Omiddezyani, E. Houshfar, S.R. Miremadi, M. Ashjaee, A.M. Nejad, Lithium-ion battery thermal management system with Al2O3/AgO/CuO nanofluids and phase change material, Appl. Therm. Eng. 180 (2020) 115840, https://doi.org/10.1016/j.applthermaleng.2020.115840.
[34] L. He, X. Tang, Q. Luo, Y. Liao, X. Luo, J. Liu, L. Ma, D. Dong, Y. Gan, Y. Li, Structure optimization of a heat pipe-cooling battery thermal management system based on fuzzy grey relational analysis, Int. J. Heat Mass Transf. 182 (2022) 121924, https://doi.org/10.1016/j.ijheatmasstransfer.2021.121924.
[35] W. Yang, F. Zhou, H. Zhou, Q. Wang, J. Kong, Thermal performance of cylindrical lithium-ion battery thermal management system integrated with mini-channel liquid cooling and air cooling, Appl. Therm. Eng. 175 (2020) 115331, https://doi.org/10.1016/j.applthermaleng.2020.115331.
[36] J. Huang, S.T. Boles, J.-M. Tarascon, Sensing as the key to battery lifetime and sustainability, Nat. Sustainability 5 (2022) 194–204, https://doi.org/10.1038/s41893-022-00859-y.
[37] K. Field, Everything You Need To Know About Tesla's New 4680 Battery Cell, in: BATTERIES, Vol. 2020, CleanTechnica, 2020.
[38] M. Kane, Tesla's 4680-type battery cell teardown, Specs Revealed, in, InsideEVs (2022).
[39] K. Tsuruta, M. Dermer, R. Dhiman, A CELL WITH A TABLESS ELECTRODE". EP3878029 (A1), 2021.
[40] T. Alam, W. Li, W. Chang, F. Yang, J. Khan, C. Li, A comparative study of flow boiling HFE-7100 in silicon nanowire and plainwall microchannels, Int. J. Heat Mass Transf. 124 (2018) 829–840, https://doi.org/10.1016/j.ijheatmasstransfer.2018.04.010.
[41] E. Abu-Nada, Effects of variable viscosity and thermal conductivity of CuO-water nanofluid on heat transfer enhancement in natural convection: Mathematical Model and Simulation (2010) https://doi.org/10.1115/1.4000440.
[42] M. Nassar, P.A. Vázquez, N. Chauris, M. Daaboul, A. Michel, C. Louste, Experimental models of the variation of HFE-7100 and HFE-7000 electric properties with temperature, IEEE Trans. Ind. Appl. 56 (2020) 4193–4199, https://doi.org/10.1109/TIA.2020.2990367.
[43] B. Çuhadaroğlu, M.S. Hacisalihoğlu, An experimental study on the performance of water-based CuO nanofluids in a plate heat exchanger, Int. Commun. Heat Mass Transfer 137 (2022) 106255, https://doi.org/10.1016/j.icheatmasstransfer.2022.106255.
[44] W. Cao, C. Zhao, Y. Wang, T. Dong, F. Jiang, Thermal modeling of full-size-scale cylindrical battery pack cooled by channeled liquid flow, Int. J. Heat Mass Transf. 138 (2019) 1178–1187, https://doi.org/10.1016/j.ijheatmasstransfer.2019.04.137.
[45] C. Zhao, W. Cao, T. Dong, F. Jiang, Thermal behavior study of discharging/charging cylindrical lithium-ion battery module cooled by channeled liquid flow, Int. J. Heat Mass Transf. 120 (2018) 751–762, https://doi.org/10.1016/j.ijheatmasstransfer.2017.12.083.
[46] H. Wang, T. Tao, J. Xu, X. Mei, X. Liu, P. Gou, Cooling capacity of a novel modular liquid-cooled battery thermal management system for cylindrical lithium ion batteries, Appl. Therm. Eng. 178 (2020) 115591, https://doi.org/10.1016/j.applthermaleng.2020.115591.
[47] Y. Gan, L. He, J. Liang, M. Tan, T. Xiong, Y. Li, A numerical study on the performance of a thermal management system for a battery pack with cylindrical cells based on heat pipes, Appl. Therm. Eng. 179 (2020) 115740, https://doi.org/10.1016/j.applthermaleng.2020.115740.
[48] D. Bernardi, E. Pawlikowski, J. Newman, A general energy balance for battery systems, J. Electrochem. Soc. 132 (1985) 5, https://doi.org/10.1149/1.2113792.
[49] Z. An, L. Jia, L. Wei, C. Dang, Q. Peng, Investigation on lithium-ion battery electrochemical and thermal characteristic based on electrochemical-thermal coupled model, Appl. Therm. Eng. 137 (2018) 792–807, https://doi.org/10.1016/j.applthermaleng.2018.04.014.
[50] Y. Lai, W. Wu, K. Chen, S. Wang, C. Xin, A compact and lightweight liquid-cooled thermal management solution for cylindrical lithium-ion power battery pack, Int. J. Heat Mass Transf. 144 (2019) 118581, https://doi.org/10.1016/j.ijheatmasstransfer.2019.118581.
[51] T.G. Tranter, R. Timms, P.R. Shearing, D. Brett, Communication—prediction of thermal issues for larger format 4680 cylindrical cells and their mitigation with enhanced current collection, J. Electrochem. Soc. 167 (2020) 160544, https://doi.org/10.1149/1945-7111/abd44f.
[52] C. Lin, H. Wen, L. Liu, S. Liu, T. Ma, B. Fan, F. Wang, Heat generation quantification of high-specific-energy 21700 battery cell using average and variable specific heat capacities, Appl. Therm. Eng. (2020) 116215, https://doi.org/10.1016/j.applthermaleng.2020.116215.
[53] A. Sarchami, M. Kiani, M. Najafi, E. Houshfar, Experimental investigation of the innovated indirect-cooling system for Li-ion battery packs under fast charging and discharging, J. Storage Mater. 61 (2023) 106730, https://doi.org/10.1016/j.est.2023.106730.
[54] C. Zhao, A.C. Sousa, F. Jiang, Minimization of thermal non-uniformity in lithium-ion battery pack cooled by channeled liquid flow, International Journal of Heat and Mass Transfer 129 (2019) 660–670, https://doi.org/10.1016/j.ijheatmasstransfer.2018.10.017.
[55] J. Liang, Y. Gan, Y. Li, Investigation on the thermal performance of a battery thermal management system using heat pipe under different ambient temperatures, Energ. Conver. Manage. 155 (2018) 1–9, https://doi.org/10.1016/j.enconman.2017.10.063.